5644 *Chem. Mater.* **2010,** *22,* 5644–5652
DOI:10.1021/cm102089c

CHEMISTRY OF MATERIALS
Article

New Insights into the Atomic Structure of 45S5 Bioglass by Means of Solid-State NMR Spectroscopy and Accurate First-Principles Simulations

Alfonso Pedone,*[,†] Thibault Charpentier,*[,‡] Gianluca Malavasi,[§] and Maria Cristina Menziani[§]

[†]*Scuola Normale Superiore, Piazza dei Cavalieri 7, Pisa, Italia,* [‡]*CEA, IRAMIS, Service Interdisciplinaire sur les Systèmes Moléculaires et Matériaux, LSDRM, UMR CEA/CNRS 3299, F-91191 Gif-sur-Yvette cedex, France, and* [§]*Dipartimento di Chimica, Università di Modena e Reggio Emilia, Via G. Campi 183, 41125 Modena, Italia*

Received July 27, 2010

An integrated computational method that couples classical molecular dynamics simulations with density functional theory calculations has been used to simulate the solid-state ^{17}O and ^{23}Na MQMAS, ^{29}Si, ^{31}P, and ^{23}Na static and MAS NMR spectra of the 45S5 Bioglass structural models with up to 248 atoms. Comparison with the experimental spectra collected in this work (the ^{17}O MQMAS spectrum of the 45S5 Bioglass is reported for the first time in the literature) shows an excellent agreement. The results provide deep insights into fundamental open questions regarding the atomic-scale structural details of this glass of great medical interest. In particular, the host silica network, described by the Q^n distribution (a Q^n species is a network-forming ion bonded to n bridging oxygens), consists of chains and rings of Q^2_{Si} (67.2%) SiO_4 tetrahedra cross-linked with Q^3_{Si} (22.3%) species and terminated by a low quantity of Q^1_{Si} (10.1%) species. No Si−O−P bridges have been detected by both ^{31}P NMR and ^{17}O MQMAS experiments, and therefore isolated orthophosphate units are able to form nanodomains that subtract sodium and calcium cations from their network modifying role into the silicate network. Finally, both the experimental and theoretical results show a mixture of dissimilar cations (Na,Ca) around NBO, according to a nonrandom distribution of these species.

Introduction

Bone and cartilage are tissues that are often in need of regeneration because of trauma, tumor removal, or more commonly, age-related diseases such as osteoporosis and osteoarthritis. As life expectancy increases and degenerative bone diseases become more common, the need for new materials that can stimulate the body's own regenerative mechanism and heal tissues is becoming urgent. To this respect, bioactive glasses show high potential medical utility.[1−5]

The 45S5 Bioglass (46.1% SiO_2, 24.4% Na_2O, 26.9% CaO, 2.6% P_2O_5, in mol %) was the first material seen to form an interfacial bond with host tissue, when implanted in rats.[6] Bioglass particulates have been in clinical use since 1993 as Perioglas, used to fill periodontal defects (USBiomaterials Corp., Alachua, Florida), and more recently as NovaBone (NovaBone Corp., Alachua, Florida), used in orthopedic applications.

A crucial factor in the gene switching mechanism needed to initiate the required osteoblast activity is the rate at which Ca, P, Si ions enter the fluid surrounding the glass.[7] This is strongly influenced by the concentration of phosphate units into the glass,[8−10] which affects the silicon topological network, the environment of the Ca and Na sites, and their distribution around oxygen ions.

Notwithstanding, several experimental and computational studies have attempted to correlate the composition of these materials with their reactivity and biological responses, the atomic-scale structural details have not been completely elucidated.

Among the standard solid-state experimental techniques, neutron and X-ray diffraction,[11] nuclear magnetic resonance (NMR),[12−15] and Raman[10,16] and infrared

*Corresponding author. E-mail: alfonso.pedone@sns.it (A.P.); thibault.charpentier@cea.fr (T.C.).

(1) Vallet-Regi, M. *J. Chem. Soc., Dalton Trans.* **2001**, 97.
(2) Jones, J. R.; Hench, L. L. *J. Biomed. Mater. Res. B: Appl. Biomater.* **2004**, *68B*, 36.
(3) Jones, J. R.; Lee, P. D.; Hench, L. L. *Philos. Trans. R. Soc. London, Ser. A* **2006**, *364*, 263.
(4) Cerruti, M.; Sahai, N. *Rev. Min. Geochem.* **2006**, *64*, 283.
(5) Hench, L. L.; Andersson, O. H. Bioactive Glasses. In *An Introduction to Bioceramics*; World Scientific: Singapore, 1993.
(6) Hench, L. L.; Splinter, R. J.; Alen, W. C.; Greenlee, T. K. *J. Biomed. Mater. Res.* **1971**, *2*, 117.
(7) Xynos, I. D.; Edgar, A. J.; Buttery, L. D.; Hench, L. L.; Polak, J. M. *J. Biomed. Mater. Res.* **2001**, *55*, 151.
(8) Clayden, N. J.; Espisito, S.; Pernice, P.; Aronne, A. *J. Mater. Chem.* **2001**, *11*, 936.
(9) Angeli, F.; Delaye, J. M.; Charpentier, T.; Petit, J. C.; Ghaleb, D.; Faucon, P. *J. Non-Cryst. Solids* **2000**, *276*, 132.
(10) Lin, C. C.; Huang, L. C.; Shen, P. *J. Non-Cryst. Solids* **2005**, *351*, 3195.
(11) FitzGerald, V.; Pickup, D. M.; Greenspan, D.; Sarkar, G.; Fitzgerald, J. J.; Wetherall, K. M.; Moss, R. M.; Jones, J. R.; Newport, R. J. *Adv. Funct. Mater.* **2007**, *17*, 3746.

 Published on Web 09/09/2010

spectroscopy[17] have been employed to probe the structural features of different bioglass compositions and to highlight the structural changes which characterize bioactivity. Moreover, from the theoretical point of view, computer simulations have become an attractive and complementary methodology to fill the gap in fundamental knowledge because of the increasingly more powerful computational methods and resources.[18,19]

The picture of the medium-range order of the 45S5 Bioglass emerging from these studies was initially characterized by a very open silicate network, mainly dominated by Q^2_{Si} and Q^3_{Si} species (a Q^n species is a network-forming ion bonded to n bridging oxygens), interspersed with isolated orthophosphate groups. This simple binary model of the silica network, traditionally inferred from MAS NMR spectra,[11,13,15,20,21] has recently been demonstrated not to be optimal for the fitting of 1D MAS NMR spectra of bioactive glasses with variable concentration of phosphourus; therefore, a ternary model with Q^1_{Si}, Q^2_{Si}, and Q^3_{Si} species has been proposed,[14] in agreement with the results of previous Raman spectra[10] and of several classical and Carr−Parrinello molecular dynamics simulations.[22−27] Moreover, recent ^{29}Si MAS NMR experiments,[14] IR and Raman data[10,16,17] and computational simulations[23−26] indicate that a small fraction of pyrophosphate (Q^1 or Si−O−P) species can coexist with the majority of orthophosphate species detected by earlier investigations.[11,13,20] This arrangement may strongly affect the phosphate release rate due to the labile nature of surface P−O−Si bridges.

Moreover, in a recent work Angelopoulou et al.[21] assigned the peak at 8 ppm in the ^{31}P MAS spectrum to pyrophosphate units, which is in contradiction with previous experimental interpretations[11,14,15] and computational studies.[18,27,28]

With the aim of gaining new insights into this contradictory description of the atomic level structure of 45S5 Bioglass, a synergic and complementary approach which combines experimental and computational techniques will be used in this paper. The ^{17}O and ^{23}Na 3QMAS NMR spectrum of the ^{17}O-enriched 45S5 Bioglass and the ^{29}Si, ^{31}P, and ^{23}Na MAS spectra of the ^{29}Si-enriched glass will be collected in this work and reported for the first time in the literature. Moreover, an integrated computational method, recently developed by us,[29] which couples classical molecular dynamics (CMD) simulations with periodic density functional theory (DFT) calculations (employing the GIPAW approach[30,31]) will be used to generate the theoretical solid-state ^{29}Si, ^{31}P, and ^{23}Na MAS and ^{17}O and ^{23}Na 3QMAS NMR spectra of this important material. Hereafter, the integrated computational method used will be named CMD/DFT-GIPAW and the adjective "theoretical" will refer to the spectra generated with this approach, in contrast to the adjective 'simulated' that is usually used for NMR spectra generated with effective NMR parameters fitted on experimental spectra. To gain good statistics, we will obtain the theoretical spectra by merging the NMR spectra of three structural models containing 248 atoms each. To the best of our knowledge, these systems are among the largest ones used to simulate NMR spectra by quantum mechanical approaches.

The theoretical spectra will be used to interpret the experimental counterparts and the calculated NMR parameters employed as starting points and boundary constraints during the direct fit of the experimental spectra.

Experimental Section

Sample Preparation. Two 45S5 Bioglass samples with theoretical molar composition of $46.2SiO_2 \cdot 24.3Na_2O \cdot 26.9CaO \cdot 2.6P_2O_5$ were prepared in ~200 mg batches by conventional melt quenching methods. The batch materials used in glass melting were high-purity quartz-SiO_2, Na_2CO_3, $CaCO_3$, and $Na_3PO_4 \cdot 12H_2O$. The powder mixture of the first sample, enriched in ^{29}Si was melted in a Pt crucible at 1350 °C by using two heating rates: 5 °C/min in the range 20−1000 and 15 °C/min above 1000 °C. The melt was refined for 2 h at the melting temperature, then quenched in air on a graphite plate mold. The ^{17}O−^{29}Si-enriched glass (second sample) was synthesized by using both ^{17}O-enriched and ^{29}Si-enriched SiO_2 precursors. This glass was melted in a flowing N_2 atmosphere to avoid loss of ^{17}O by isotopic exchange with oxygen in air. All glass samples were completely transparent and colorless showing no visual indication of phase separation. The chemical compositions of all glasses were analyzed by SEM-EDS (scanning electron microscopy equipped with energy dispersive spectrometer); the results reproduce very well (< 2%) the theoretical molar compositions.

MAS and MQMAS NMR Spectra. NMR data have been collected on Bruker Avance 300WB and 500 WB spectrometers, using Bruker CPMAS Probes (4 mm rotor) at a spinning frequency of 12.5 kHz.

(12) Clayden, N. J.; Pernice, P.; Aronne, A. *J. Non-Cryst. Solids* **2005**, *351*, 195.
(13) Elgayar, I.; Aliev, A. E.; Bocaccini, A. R.; Hill, R. G. *J. Non-Cryst. Solids* **2005**, *351*, 173.
(14) Linati, L.; Lusvardi, G.; Malavasi, G.; Menabue, L.; Menziani, M. C.; Mustarelli, P.; Pedone, A.; Segre, U. *J. Non-Cryst. Solids* **2008**, *354*, 84.
(15) Brauer, D. S.; Karpukhina, N.; Law, R. V.; Hill, R. G. *J. Mater. Chem.* **2009**, *19*, 5629.
(16) Oliveira, J. M.; Correia, R. N.; Fernandes, M. H. *Biomaterials* **2002**, *23*, 371.
(17) ElBatal, H. A.; Azooz, M. A.; Khalil, E. M. A.; Soltan Monem, A.; Hamdy, Y. M. *Mater. Chem. Phys.* **2003**, *80*, 599.
(18) Tilocca, A. *Proc. R. Soc. London, Ser. A* **2009**, *465*, 1003.
(19) Pedone, A. *J. Phys. Chem. C* **2009**, *113*, 20773.
(20) Lockyer, M. W. G.; Holland, D.; Dupree, R. *J. Non-Cryst. Solids* **1995**, *188*, 207.
(21) Angelopoulou, A.; Montouillout, V.; Massiot, D.; Kordas, G. *J. Non-Cryst. Solids* **2008**, *354*, 333.
(22) Tilocca, A.; Cormack, A. N.; de Leeuw, N. H. *Chem. Mater.* **2007**, *19*, 95.
(23) Tilocca, A. *Phys. Rev. B* **2007**, *76*, 224202.
(24) Tilocca, A. *J. Chem. Phys.* **2008**, *129*, 084504.
(25) Corno, M.; Pedone, A.; Dovesi, R.; Ugliengo, P. *Chem. Mater.* **2008**, *20*, 5610.
(26) Corno, M.; Pedone, A. *Chem. Phys. Lett.* **2009**, *476*, 218.
(27) Pedone, A.; Malavasi, G.; Menziani, M. C. *J. Phys. Chem. C* **2009**, *113*, 15723.
(28) Malavasi, G.; Menziani, M. C.; Pedone, A.; Civalleri, B.; Corno, M.; Ugliengo, P. *Theor. Chem. Acc.* **2007**, *117*, 933.
(29) Pedone, A.; Charpentier, T.; Menziani, M. C. *Phys. Chem. Chem. Phys.* **2010**, *12*, 6054.
(30) Ashbrook, S. E.; Berry, A. J.; Frost, D. J.; Gregorovic, A.; Pickard, C. J.; Readman, J. E.; Wimperis, S. *J. Am. Chem. Soc.* **2007**, *129*, 13213.
(31) Profeta, M.; Mauri, F.; Pickard, C. J. *J. Am. Chem. Soc.* **2003**, *125*, 541.

^{29}Si and ^{31}P static (i.e., non−spinning) MAS NMR spectra have been acquired on the 300WB spectrometer (magnetic field 7.02T) using a single pulse sequence with a recycle delay of 4s (1024 scans) and 30s (128 scans) respectively (no change in line shape was observed for longer recycle delay). Chemical shifts are referenced to secondary external samples of powder tetrakis-(trimethylsilyl)silane (which highest-intensity peak is situated −9.9 ppm from that of TMS) and hydroxyapatite $Ca_5(PO_4)_3$-(OH) (2.8 ppm from ^{31}P in H_3PO_4).

^{17}O and ^{23}Na MAS and MQMAS NMR spectra have been collected on the 500WB spectrometer (magnetic field 11.72T). For the ^{17}O Triple Quantum MQMAS spectrum, a Z-filter pulse sequence[32] has been used. 90 increments of 80 us in the first dimension with 5400 FID's per t_1 were collected with a recycle delay of 1 s. For the ^{23}Na triple quantum MQMAS spectrum, the highest signal-to-noise ratio was obtained with a two-pulse sequence involving a rotational induced adiabatic coherence transfer (RIACT) for second pulse,[33] 128 increments of 10 μs in the first dimension with 108 FID's per t_1 were collected with a recycle delay of 0.5 s. ^{17}O MQMAS data have been processed using an home-build software, as described in ref 9, whereas an inversion approach has been applied to treat the ^{23}Na MQMAS data.[9]

Computational Approach. Three models of the 45S5 Bioglass were generated by means of classical molecular dynamics simulations by using the core−shell interatomic potential recently parametrized by Tilocca et al.[22,34] This potential has been shown to reproduce better the medium range order in phospho-silicate glasses with respect to a simpler rigid ionic model.[24] The initial configurations were generated by placing randomly 248 atoms in a cubic box of 14.86 Å accordingly to the experimental density of 2.66 g/cm^3. The systems were heated and hold at 3200 K for 100 ps in the NVT ensemble ensuring a suitable melting of the samples. The liquids were then cooled to 300 K at a nominal cooling rate of 10 K/ps. The resulting glass structures were subjected to a final NVT trajectory of 200 ps. The leapfrog algorithm encoded in the DLPOLY package[35] has been used to integrate the equation of motions by using a time step of 0.2 fs. This leaded to fluctuations of less than 0.005% and no overall drift in the total energy.

NMR calculations were carried out with the CASTEP[36] density functional theory (DFT) code using the GIPAW[30] algorithm, which allows the reconstruction of the all electron wave function in the presence of a magnetic field. The generalized gradient approximation (GGA) PBE[37] functional was employed, and the core−valence interactions were described by ultrasoft pseudopotentials.

For ^{17}O, the 2s and 2p orbitals were considered as valence states with a core radius of 1.3 A; for ^{29}Si and ^{31}P, a core radius of 1.8 Å was used with 3s and 3p valence orbitals; for ^{23}Na, a core radius of 1.3 Å was used with 2s, 2p, and 3s valence orbitals, whereas for ^{43}Ca, a core radius of 2.0 Å was used with 3s, 3p, and 4s valence states. It has been previously demonstrated that in the DFT approximation, the energy of Ca 3d orbitals is too low and the hybridization with O 2p orbitals is overestimated. As a consequence, the ^{17}O chemical shifts computed with PBE are affected by very large errors (up to 124 ppm) for O sites close to Ca atoms. As shown by Profeta et al.[38] this error can be efficiently corrected by shifting the energy level of the Ca 3d orbitals in the pseudopotential generation by a constant value of +3.2 eV . This shift was found to be transferable to very different Ca and O environments.[39] Thus, in the present calculations, a modified Ca pseudopotential with shifted 3d orbitals was used, according to ref 38.

Wave functions were expanded in plane waves with the kinetic energy cutoff of 700 eV. Before computing the NMR parameters, constant volume geometry optimizations of the classical generated models were performed using a 2 × 2 × 2 Monkhorst-Pack k-point grid.[40] After optimizations, forces less than 50 meV/A were observed.

The NMR shielding tensor, $\vec{\sigma}(\mathbf{r})$ is defined as $\mathbf{B}_{in}(\mathbf{r}) = \vec{\sigma}(\mathbf{r})\mathbf{B}$, where $\mathbf{B}$ is an external uniform magnetic field and $\mathbf{B}_{in}(\mathbf{r})$ is the induced nonuniform magnetic field. The isotropic chemical shift $\delta_{iso}(\mathbf{r})$ for a nucleus in the position $\mathbf{r}$ is obtained from the isotropic chemical shielding $\vec{\sigma}_{iso}(\mathbf{r}) = \frac{1}{3}Tr\{\vec{\sigma}(r)\}$ through $\delta_{iso}(\mathbf{r}) = -[\vec{\sigma}_{iso}(\mathbf{r}) - \sigma_{ref}]$, where σ_{ref} is the isotropic shielding of the same nucleus in a reference system. In this work, to fix the ^{17}O, ^{29}Si, and ^{31}P δ scale the values of 260.5, 322.1, and 278.8 ppm have been used for $\sigma_{ref.}$ These values have been obtained by α-cristobalite, α-quartz, and $AlPO_4$ berlinite, respectively. The experimentally determined quadrupolar moment, eQ, of 25.58 and 104 mB were used for the ^{17}O and ^{23}Na atoms.[41]

The simulation of the solid-state ^{29}Si, ^{31}P, static, MAS, and ^{17}O 3QMAS NMR spectra from the CASTEP outputs have been carried out by means of a homemade software named fpNMR.[9,29] For each atomic site i, the NMR spectrum of interest, say $I_i(\vec{v})$, is calculated and then coadded to yield the final NMR spectra $I(\vec{v}) = \Sigma_i I_i(\vec{v})$. The software allows the summation to be restricted to a given chemical speciation of the considered atom and to merge the spectra of several structural model to increase the statistical data. A Floquet theorem-based formalism was used to perform NMR spectra simulation from the GIPAW NMR parameters as described in refs 9 and 29.

Results and Discussion

^{29}Si and ^{31}P NMR Spectra. The experimental ^{29}Si MAS NMR spectrum of the ^{29}Si-enriched 45S5 Bioglass (collected at 7.05T) is shown in Figure 1. It exhibits a slightly asymmetric peak with fwhm of 12 ppm, which is narrower with respect to those previously reported by FitzGerald et al.[11] (fwhm = 16 ppm) and Linati et al. (fwhm = 14 ppm). A deconvolution scheme by Gaussian fitting into two or three peaks is commonly used for the interpretation of the spectrum in terms of Q^n units describing the connectivity of the TO_4 tetrahedra that make up the structure. FitzGerald et al.,[11] by fitting the ^{29}Si spectrum with two Gaussians centered at −80.4 and −88.1 ppm to represent Q^2_{Si} and Q^3_{Si} units, respectively, estimated a binomial Q^n_{Si} distribution composed of 69% Q^2_{Si} and 31% Q^3_{Si} units. A binomial distribution was also assumed by Angelopoulou et al.,[21] who

(32) Amoureux, J. P.; Fernandez, C.; Steuernagel, S. *J. Magn. Reson.* **1996**, *123*, 116.
(33) Wu, G.; Rovnyak, D.; Griffin, R. G. *J. Am. Chem. Soc.* **1996**, *118*, 9326.
(34) Tilocca, A.; de Leeuw, N. H.; Cormack, A. N. *Phys. Rev. B* **2006**, *73*, 104209.
(35) Smith, W.; Forester, T. R. *J. Mol. Graphics* **1996**, *14*, 136.
(36) Segall, M. D.; Lindan, P. J. D.; Probert, M. J.; Pickard, C. J.; Hasnip, P. J.; Clarck, S. J.; Payne, M. C. *J. Phys.: Condens. Matter* **2002**, *14*, 2717.
(37) Perdew, J. P.; Burke, K.; Ernzerhof, M. *Phys. Rev. Lett.* **1996**, *77*, 3865.
(38) Profeta, M.; Benoit, M.; Mauri, F.; Pickard, C. J. *J. Am. Chem. Soc.* **2004**, *126*, 12628.
(39) Gervais, C.; Laurencin, D.; Wong, A.; Pourpoint, F.; Labram, J.; Woodward, B.; Howes, A. P.; Pike, K. J.; Dupree, R.; Mauri, F.; Bonhomme, C.; Smith, M. E. *Chem. Phys. Lett.* **2008**, *464*, 42.
(40) Monkhorst, H.; Pack, J. D. *Phys. Rev. B* **1976**, *13*, 5188.
(41) Pyykkö, P. *Mol. Phys.* **2008**, *106*, 1965.

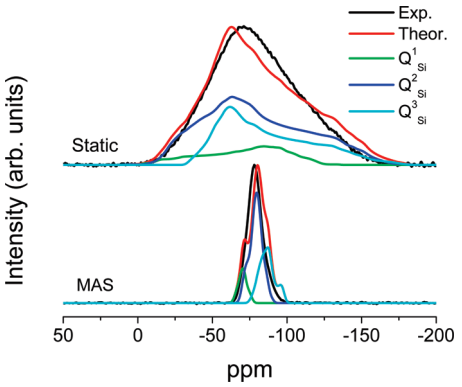

Figure 1. Comparison between experimental (black lines) and theoretical (colors) ^{29}Si static and MAS NMR spectra, at a magnetic field of 7.05 T. Individual spectra are scaled to the same maximum height.

centered the Q^2_{Si} and Q^3_{Si} peaks at −79.5 and −83.1 ppm. By contrast, the best fit obtained by Linati et al.[14] was due to a trinomial distribution with the peaks of Q^1_{Si} (15.0%), Q^2_{Si} (67.0%), and Q^3_{Si} (18.0%) species centered at −78.0, −82.0, and −88.0 ppm, respectively. A trinomial distribution is supported by several classical molecular dynamics simulations using the shell-model potential and Car−Parrinello molecular dynamics simulations.[18,19,23,27] However, computer simulations approaches seem to underestimate the fraction of Q^2 species, which commonly converges at a value of 53%. In fact, the three-dimensional structural CMD model obtained in this paper by means of classical molecular dynamics simulations presents a Q^n_{Si} distribution of 12.2, 54.5, and 33.3% of Q^1_{Si}, Q^2_{Si} and Q^3_{Si} species, in good agreement with those previously determined.

The theoretical ^{29}Si static and MAS NMR spectra generated from this structural model are superimposed to the experimental ones in Figure 1. The theoretical spectra are obtained by the fpNMR code,[29] using the NMR parameters derived from the CMD/DFT-GIPAW calculations (see Table 1). An encouraging agreement is observed. In particular, the position of maximum at −79.0 ppm in the MAS spectrum compares very well to the experimental one which is centered at −78.0 ppm. The detailed inspection of the different Q^n contributions (Figure 1) shows that the peaks of the Q^1_{Si}, Q^2_{Si}, and Q^3_{Si} species are rather overlapped, thus underlining the difficulty encountered by the use of a least-squares fitting procedure of the 1D NMR spectrum without additional constraints.

The mean values and standard deviations of the theoretical ^{29}Si NMR parameters for the different Q^n species are listed in Table 1. The average values of ^{29}Si isotropic chemical shifts (δ_{iso}) of Q^2 and Q^3 species are −79.5 and −87.0 ppm, in agreement with those used by FitzGerald et al.,[14] whereas the average δ_{iso} of Q^1 species is −70.7 ppm, which lies in the range from −69.0 to −74.0 ppm as found in typical silicate glasses.[42,43]

Therefore, these results provide a further evidence of the fact that a trinomial distribution is fully compatible with the experimental ^{29}Si NMR spectra and that the magnetic parameters calculated with the CMD/DFT-GIPAW approach can be safely used to constrain the deconvolution of the experimental spectra as it will be shown below.

Table 1. Structural Features and Computed NMR Parameters of Silicon and Phosphorous Network Formers (standard deviations are reported in parentheses)

	Silicon			Phosphorus	
	Q^1	Q^2	Q^3	Q^0	Q^1
percentage	12.2	54.5	33.3	73.3	26.7
⟨T−O⟩	1.65(0.01)	1.64(0.01)	1.64(0.01)	1.55(0.01)	1.56(0.01)
⟨Si−O−T⟩	134.1(7.3)	136.4(7.6)	135.1(6.8)		125.9(8.9)
δ_{iso}	−70.7(2.7)	−79.5(4.2)	−87.0(5.2)	8.7(6.3)	−0.7(10.1)
Δ_{CS}	53.7(27.6)	−73.0(13.8)	−66.7(14.0)	−11.2(28.1)	−70.2(10.6)
η_{CS}	0.54(0.21)	0.61(0.13)	9.25(0.16)	0.71(0.26)	0.41(0.10)

Table 2. CMD/DFT-GIPAW NMR Parameters and Population of Oxygen Speciation (standard deviations are reported in parentheses)

	δ_{iso} (ppm)	C_Q (MHz)	η_Q	population (%)
NBO	96.5(24.9)	3.20(0.99)	0.30(0.18)	67.0
P−O(Ca,Na)	122.9(12.4)	5.06(0.32)	0.18(0.10)	11.0
P−O(Na)	100.5(14.6)	4.93(0.27)	0.10(0.06)	1.0
P−O(Ca)	140.4(17.1)	5.09(0.55)	0.25(0.16)	1.0
Si−O(Ca,Na)	92.5(17.5)	2.72(0.33)	0.34(0.18)	44.0
Si−O(Na)	52.0(9.2)	2.80(0.31)	0.27(0.15)	3.0
Si−O(Ca)	120.8(12.6)	2.74(0.25)	0.30(0.17)	6.0
BO	74.9(11.3)	4.80(0.53)	0.42(0.22)	33.0
Si−O−Si	73.7(8.8)	4.76(0.48)	0.42(0.21)	32.0
Si−O(Ca,Na)−Si	80.3(7.7)	4.59(0.49)	0.47(0.25)	8.0
Si−O(Na)−Si	71.2(8.0)	4.83(0.46)	0.39(0.19)	22.0
Si−O(Ca)−Si	73.8(8.7)	4.70(0.53)	0.48(0.25)	2.0
P−O−Si	115.7(10.6)	6.14(0.28)	0.55(0.26)	1.0
P−O(Ca,Na)−Si	118.3(9.6)	6.08(0.39)	0.64(0.26)	0.5
P−O(Na)−Si	113.1(14.7)	6.20(0.26)	0.46(0.33)	0.5

A second structural factor that might influence the ^{29}Si isotropic chemical shift δ_{iso} is the mean ⟨Si−O−T⟩ angle, where T denotes a connected tetrahedron. The correlation between the theoretical ^{29}Si isotropic chemical shift δ_{iso} (Table 2) and the mean $<$Si−O−T$>$ θ angle for the glass studied is reported in Figure 2. Linear regression analysis of the data as $\theta = a\delta_{iso} + b$ points yields slopes of −1.1791, −1.0721, and −1.487 with correlation coefficients R^2 of 0.55, 0.62, and 0.887 for Q^1_{Si}, Q^2_{Si}, and Q^3_{Si} species, respectively. Thus, the best correlation is found for the Q^3_{Si} species; this might be ascribed to the lower number of Ca ions (1.6) surrounding the Q^3_{Si} species with respect to Q^2_{Si} (2.7) and Q^3_{Si} (4.0), the number of Na ions around the different Q^n sites being almost constant (4.4, 4.6, and 4.9 for Q^1_{Si}, Q^2_{Si} and Q^1_{Si}, respectively). In fact, other structural parameters could contribute to the ^{29}Si chemical shifts of Si species embedded in a rich Ca environment, due to the partial covalent character of the Ca−O bond which comes from the hybridization between the Ca 3d orbitals and the O 2p orbitals.[38] Accordingly, similar correlations have been previously obtained for the $CaSiO_3$ glass,[29] whereas better correlation coefficients were obtained for sodium and lithium silicate glasses.[9,44]

Therefore, the nonrandom distribution of Na and Ca around oxygen atoms in the glass (see below) seems to control the Q^n_{Si} distribution.

(42) De Jong, B. H. W. S.; Schramm, C. M.; Parziale, V. E. *J. Am. Chem. Soc.* **1984**, *106*, 4396.
(43) Zhang, P.; Grandinetti, P. J.; Stebbins, J. F. *J. Phys. Chem. B* **1997**, *101*, 4004.
(44) Clarck, T. M.; Grandinetti, P. J. *Solid State NMR* **2005**, *27*, 233.

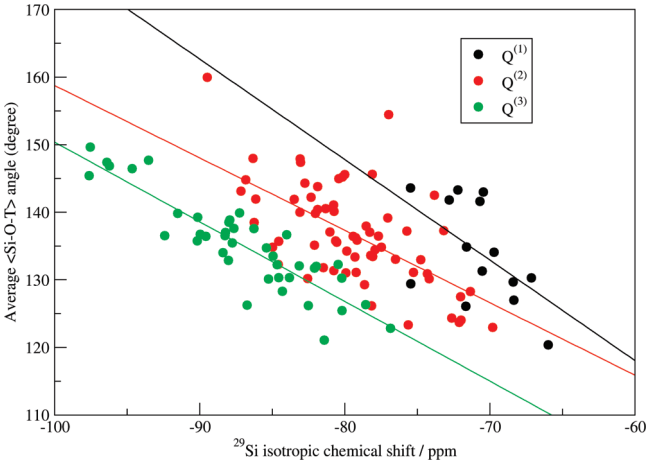

Figure 2. Computed ^{29}Si isotropic chemical shift as a function of the mean ⟨Si−O−T⟩ angle.

The experimental ^{31}P MAS NMR spectrum, reported in Figure 3, shows one broad peak at 8.7 ppm assigned to isolated orthophosphate units which coordinate modifier cations subtracting them from the silicate network. This figure also reports the theoretical spectrum of the three-dimensional structural CMD model obtained in this work, it presents 73.3 and 26.7% of Q^0_P and Q^1_P units, respectively. Although the CMD simulations has been carried out with 248 atoms (see Methods Section) the result obtained is very similar to the values (Q^0_P = 80.0%) obtained by CMD simulations with thousands of atoms in the simulation box.[24,27] The theoretical spectrum shows that the peak of the Q^1_P species is shielded by 9.4 ppm with respect to that of the Q^0_P because of the interconnection of the PO_4^{3-} and SiO_4^{4-} units. This is clearly distinguishable in the theoretical MAS spectrum, and clearly absent in the experimental one.

Interestingly, Table 1 shows that the chemical shift anisotropy of the Q^1_P units (−70.2 ppm) is much greater than the one calculated for Q^0_P units (−11.2 ppm). Therefore, the Q^1_P signal should be very well distinguishable in the static NMR spectra (see Figure 3). However, even in this case, the disagreement between the theoretical and the experimental spectra strongly indicate that the great majority of the P atoms, if not the totality, is present as isolated orthophosphate units.

As mentioned above, the presence of Si−O−P bonds and Q^1_P speciation have been suggested by both classical and Car−Parrinello Molecular dynamics simulations and by FTIR measurements on sol gel derived Bioglass.[45] In the latter case, these features might be present on the surface of the material only and their instability when exposed to atmospheric moisture do not allow their detection by optical spectroscopic techniques.[46]

In conclusion, the combined experimental/computational approach undertaken in this work suggests that no P−O−Si bonds are present in the melt-derived Bioglass.

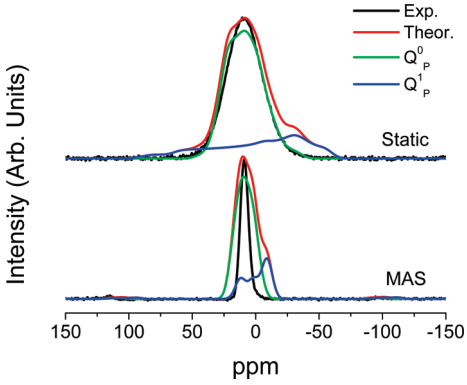

Figure 3. Comparison between experimental (black lines) and theoretical static and MAS ^{31}P NMR spectra, at magnetic field of 7.05 T. The theoretical ^{31}P static and MAS spectra have been shifted (of 8.6 ppm) so that the maximum peak of the Q^0 speciation coincides with the one of the experimental spectrum.

Direct Fitting of the Experimental ^{29}Si MAS Spectrum. By assuming that all phosphorus is present as orthophosphate units, it is possible to quantify the Si−NBO/Si−BO−Si ratio and to use it as a constraint for the Q^n distribution as follows:

$$\frac{\text{Si}-\text{NBO}}{\text{Si}-\text{BO}-\text{Si}} = \frac{(3Q^1 + 2Q^2 + Q^3)}{(0.5Q^1 + Q^2 + 1.5Q^3)} \qquad (1)$$

Using the Si−NBO/Si−BO−Si ratio (1.77) provided by the glass composition, the following equation can be obtained (see the Supporting Information for its derivation)

$$Q^1 = -0.1087Q^2 + 0.789Q^3 \qquad (2)$$

This equation has been used as constraint to fit the experimental ^{29}Si MAS spectrum using the NMR parameters obtained from the CMD/DFT-GIPAW calculations (as starting values) and mixed Gaussian−Lorentzian lineshapes (see Figure 4). This yields 10.5% of Q^1_{Si} species (centered at −71.1 ppm with fwhm = 6.0 ppm), 67.2% of Q^2_{Si} species (centered at −78.0 ppm with fwhm = 7.6 ppm), and 22.3% of Q^3_{Si} species (centered at −85.3 ppm with fwhm = 9.6 ppm).

The goodness of the fit was measured as the ratio $\rho = \sqrt{\frac{\chi^2}{\sigma^2}}$, where χ^2 is the standard chi-square error measurement and σ^2 is the standard deviation of the noise. The very high signal-to-noise ratio of our ^{29}Si MAS spectrum enabled us to investigate the sensitivity of the fit to a binomial or trinomial distribution. Hence, ρ was calculated for all possible Q^n (monomial, binomial or trinomial) distribution. For each calculation, the relative population of the Q^n species was kept constant, whereas its NMR parameters (peak position and width) were optimized through a least-squares minimization procedure. The results are displayed in Figure 5 using a ternary diagram representation. The dashed lines encompass the region of Q^n distributions yielding a ρ value that deviates from the global minimum ρ_{min} less than 5%. This diagram points out that even in the case of very high S/N spectrum the ^{29}Si MAS NMR spectrum alone cannot determine accurately the Q^n distribution. The solid line represents the compositional

(45) Cerruti, M.; Magnacca, G.; Bolis, V.; Morterra, C. *J. Mater. Chem.* **2003**, *13*, 1279.
(46) Cerruti, M.; Bianchi, C. L.; Bonino, F.; Damin, A.; Perardi, A.; Morterra, C. *J. Phys. Chem. B* **2005**, *109*, 14496.

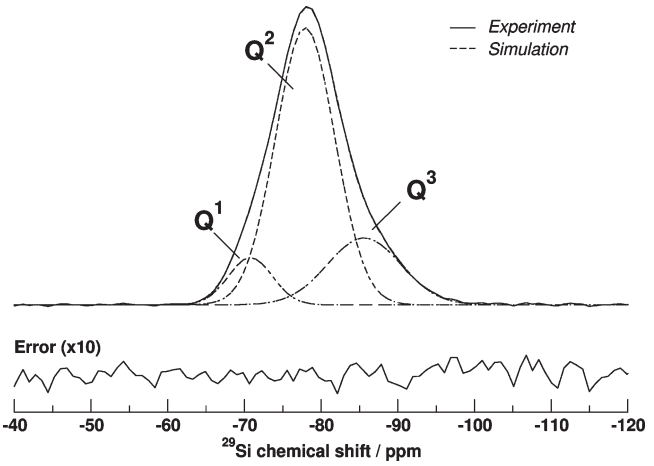

Figure 4. Fit of the experimental ^{29}Si MAS NMR spectrum constrained by using eq 2 (see text).

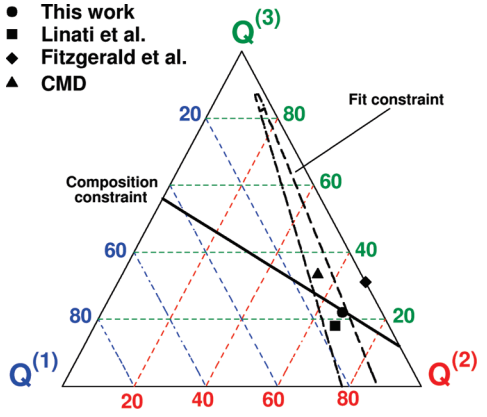

Figure 5. Ternary diagram representation of the ^{29}Si NMR spectrum fit. Dashed lines encompass the region of Q^n for which the ^{29}Si MAS NMR spectrum can be fitted with an error less that 5% above the global minimum ρ_{min} = 0.994. The solid line represents the constraint from the composition (eq 2) which yields a constrained minimum of ρ = 1.053.

constraint (eq 2), which is indeed crucial to determine the Q^n distribution. As already mentioned, our measurement is close to that of Linati et al. (15.0, 67.0, and 18.0 for Q^1_{Si}, Q^2_{Si}, and Q^3_{Si} species, respectively) and clearly corroborate the trinomial distribution. No attempt was made to derive similar compositional constraints when P−O−Si bonds are present, but the CMD point shows that the accessible region for Q^n distribution in such a general case is the upper part of the ternary diagram.

^{17}O MQMAS Spectrum. Further information on the structural units constituting the network and the nature of cation mixing and ordering around nonbridging oxygens (NBO) and bridging oxygens (BO) can be gained by analyzing the ^{17}O 3QMAS spectrum generated by the CMD/DFT-GIPAW approach and reported in Figure 6a, together with the experimental one (Figure 6b) measured for the first time in this work. The excellent agreement between the two highlights the high accuracy of the simulation and allows the interpretation of the experimental spectrum by means of the contribution of different T−NBO(modifier) and T−BO(modifier)−T structural units (Figure 6c−f).

The comparison between the theoretical and experimental spectra (panels c,d) shows that the population of bridging oxygens surrounded by sodium within a cutoff of 3.2 Å, denoted Si−BO(Na)−Si, (22% in the present CMD three-dimensional structural models) is much greater than those of the Si−BO(Ca,Na)−Si and Si−BO(Ca)−Si (8 and 2% respectively); therefore BOs prefer to be surrounded by sodium ions rather than calcium. Conversely, Si−NBO(Ca,Na), Si−NBO(Na), and Si−NBO(Ca) structural units (panels e and f) are all presented in the Bioglass with the theoretical populations being 44, 3, and 6%, respectively.

On the contrary, only P−NBO(Ca,Na) and P−NBO(Na) structural units are present in the structure.

In fact, the analysis of Figure 6d clearly shows that the signal of Si−O−P bonds, the population of which amounts to 1% in the three-dimensional CMD structural model, is not detectable in the experimental ^{17}O 3QMAS spectra (in Figure 6d: the Si−O−P signal has been multiplied by 10 for making it visible).

The computed NMR parameters (δ_{iso},C_Q,η_Q) and the population of the T−NBO and T−BO−T structural units are reported in Table 2. These values have been used to guide the fitting of the experimental ^{17}O 3QMAS spectrum for resolving and quantifying the different structural units present in the glass by using a new methodology recently introduced by some of us.[47]

The results of this fitting procedure is displayed in Figure 7, whereas the NMR parameters and site populations extracted by the fitting procedure are reported in Table 3. A very good agreement between the experimental and simulated ^{17}O 3QMAS spectra is obtained (Figure 7a). Figure 7b displays the distribution of NMR parameters of each site in the plane of the isotropic chemical shift and the quadrupolar coupling constants together with the CMD/DFT-GIPAW average values (Table 2). The good agreement found shows that CMD/DFT-GIPAW simulations allow a significant improvement in the constraint fit of complex spectra very difficult to interpret, such as the one for 45S5 Bioglass.

From this analysis emerges that the glass is constituted by 28.1% Si−BO−Si sites, 20.6% P−NBO sites composed by 5.9% and 14.7% of P−NBO(Na) and P−NBO(Ca,Na), respectively and 50.9% of Si−NBO sites, composed by 7.1, 37.3 and 6.5% of Si−NBO(Ca), Si−NBO(Ca,Na) and Si−NBO(Na) sites, respectively. Si−BO−Si could not be fitted by Si−BO(Na)−Si, Si−BO(Na,Ca)−Si, and Si−BO(Ca)−Si contributions because of insufficient resolution. The populations of the different structural units obtained by direct fit are compared to those calculated for a random distribution (see the Supporting Information for calculation details) of Na and Ca around oxygen atoms. The data values, listed in Table 3, show that,with respect to a homogeneous distribution, the first coordination shell of Si−NBO sites is depleted in

(47) Angeli, F.; Charpentier, T.; Gaillard, M.; Jollivet, P. *J. Non-Cryst. Solids* **2008**, *354*, 3713.

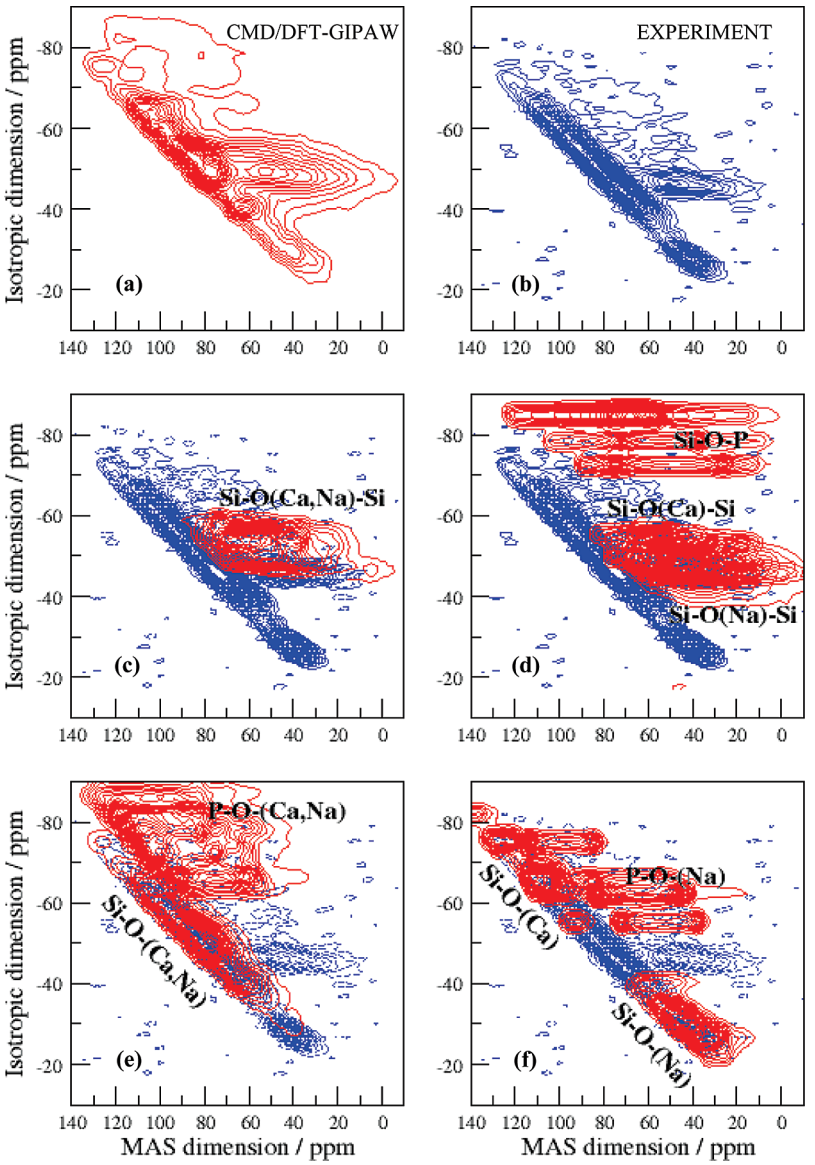

Figure 6. Comparison between the experimental (blue lines) and theoretical (red lines) ^{17}O MQMAS spectrum at a magnetic field of 11.75 T. The theoretical (a) and experimental spectra (b) have been normalized, therefore they present the same height at maximum and the contour plots are free of signal noise.

Na ions to the advantage of Ca ions, whereas the contrary happens for P−NBO sites, which present a mixture of dissimilar cations (Na,Ca).

^{23}Na MAS and MQMAS Spectra. The experimental ^{23}Na MAS NMR spectra collected at 11.75 T is reported in Figure 8. This is composed of a single broad asymmetric line centered at −3.5 ppm with a steep low-field edge and a trailing high-field edge which is linked to the distribution of electric field gradient (EFG) at the sodium site, and is typical of disordered solids. On the basis of experimental data only FitzGerald et al[11] suggested a 6-fold coordination environment within a pseudo-octahedral NaO_6 arrangement. These data are usually interpreted by reference to knowing crystalline systems and the correlation between different coordination environments and ^{23}Na NMR chemical shifts. In fact, chemical shift of ca. −50, −21, and −3 ppm are assigned to 4-, 5-, and 6-coordinated sodium ions. Insights on the signals associated to different coordination environments can be gained by looking at the simulated spectrum also reported in Figure 8. This is in good agreement with the experimental data and shows that three overlapping peaks associated to 5-, 6-, and 7-fold coordinated Na ions contribute to the total spectra, thus underlining the difficulty of the least-squares fitting procedure of the MAS NMR spectrum.

The structural model of the 45S5 Bioglass generated by means of MD simulations reveals that on average sodium is coordinated by 6.1 oxygen ions in pseudo-octahedral environment. Although the coordination number distribution has a majority (39%) of 6-fold Na ions, 24% of Na ions are 5-fold coordinated and 32% are 7-fold coordinated.

The average NMR parameters of ^{23}Na in different coordination environments calculated with the MD-GIPAW approach are reported in Table 4, from which it can be seen that the quadrupolar coupling constant decreases with the coordination number as well as the isotropic chemical shifts while the asymmetry parameter increases.

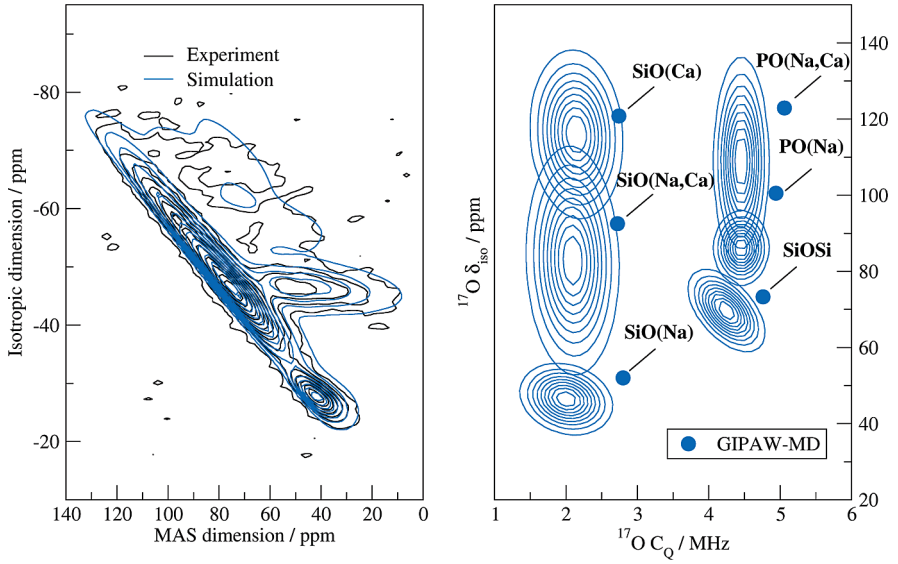

Figure 7. Left, experimental (black lines) and simulated ^{17}O MQMAS spectra using 3D NMR parameter distribution as described in the text. Right, (C_Q, δ_{iso}) 2D projection of the 3D NMR parameter distribution as obtained from the fit of the experimental data.

Table 3. NMR Parameters and Population of Oxygen Speciation Extracted from the Fitting of the Experimental ^{17}O 3QMAS Spectraa

	Δ_{iso} (ppm)	C_Q (MHz)	η_Q	population of oxygen speciation (%)	random population (%)
P−O(Ca,Na)	109.0 (12.7)	4.5 (0.2)[a]	0.30 (0.20)[b]	14.7	9.4
P−O(Na)	87.0 (4.4)	4.5 (0.2)[a]	0.30 (0.20)[b]	5.9	3.2
P−O(Ca)					0.7
Si−O(Ca,Na)	82.8 (14.3)	2.3 (0.3)	0.37 (0.05)[c]	37.3	39.3
Si−O(Na)	46.4 (4.6)	2.2 (0.3)	0.37 (0.05)[c]	6.5	13.3
Si−O(Ca)	116.0 (10.3)	2.3 (0.3)	0.37 (0.05)[c]	7.1	2.8
Si−O−Si	69.0 (5.8)	4.3 (0.4)	0.50 (0.20)	28.1	31.3
Si−O(Ca,Na)Si					11.3
Si−O(Na)Si					13.7
Si−O(Ca)Si					5.9

[a] Standard deviations are reported in parentheses. Parameters with the same exponent were constrained to have the same values. In the last column, the site population calculated for a random distribution is reported.

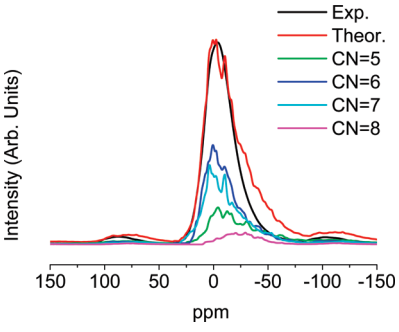

Figure 8. Experimental (black line) and theoretical (red line) ^{23}Na MAS NMR spectra of 45S5 Bioglass at 11.75 T. The theoretical spectra of 5-, 6-, 7-, and 8-fold coordinated Na ions are also reported.

The three sodium sites not distinguishable in the MAS spectrum can be better resolved with 3QMAS experiments, the spectrum of which is reported in Figure 9a.

A deconvolution of the ^{23}Na MQMAS spectrum into three components was proposed by Angelopoulou et al.[21] who detected a narrow signal with a weak quadrupolar coupling constant (δ_{iso} = 6.6 ppm and C_Q = 1.2 MHz), and two broad components with similar mean values (6.0 ppm and 6.8 ppm, respectively) and identical widths

Table 4. Theoretical (MD-GIPAW) ^{23}Na NMR Parameters and Average Na−O Bond Length Coordinated to Oxygens (CN_O)

CN_O	population	⟨Na−O⟩ (Å)	δ_{iso} (ppm)	C_Q (MHz)	η_Q	P_Q
5	0.24	2.44	13.2	5.03	0.50	5.26
6	0.39	2.51	9.5	3.56	0.58	3.78
7	0.32	2.59	9.7	3.59	0.58	3.82
8	0.06	2.66	4.9	4.49	0.44	4.64
average		2.53	10.2	4.03	0.55	4.26

(20 ppm) for the isotropic chemical shift distribution but different quadrupolar coupling constant (1.4 and 2.6 MHz, respectively).

As shown in Figure 9a, our experimental ^{23}Na MQMAS spectrum does not exhibit such a narrow component that could be related to moisture contamination of previous samples. Through the use of an inversion procedure,[9] a broad distribution of (C_Q, δ_{iso}) can be extracted from the experimental spectrum, with a small trend of a positive slope (i.e., δ_{iso} increases in average with C_Q increasing) to which the MD-GIPAW compare very well Figure 9b. Taking into account the oxygen coordination number, a comparison between experimental and MD-GIPAW (Figure 9c,d) suggests that 6−7-fold are the most probable

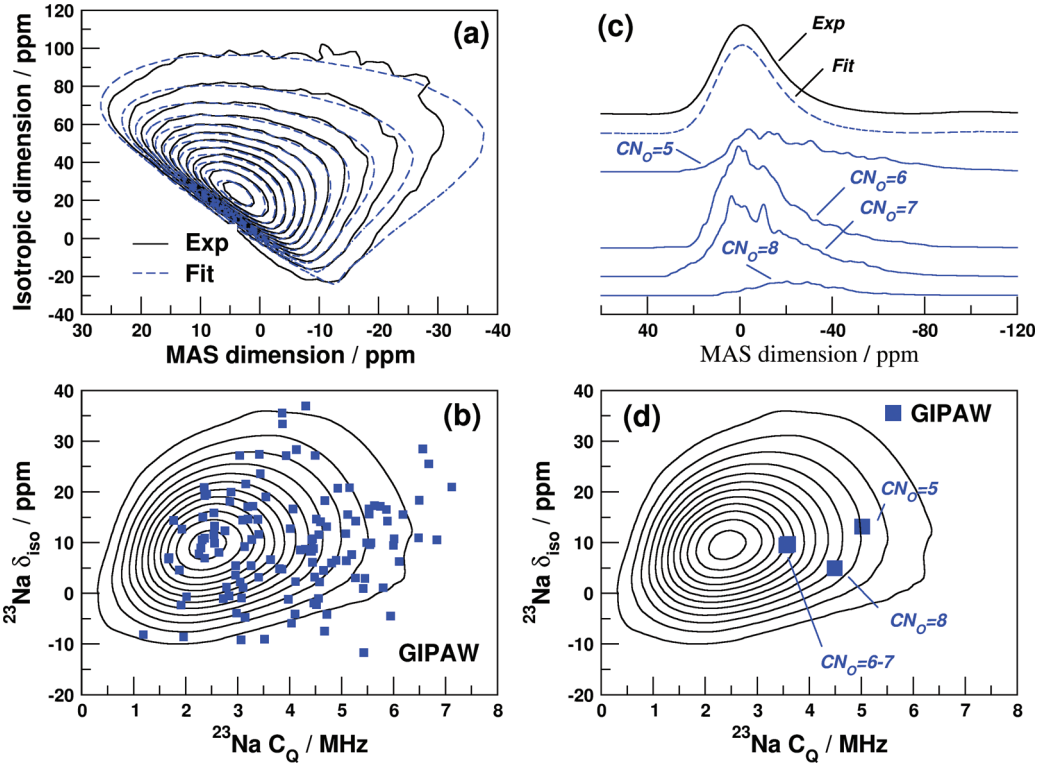

Figure 9. (a) Contour plots of the experimental and simulated ^{23}Na MQMAS spectra. (b, d) Contour plot of the two-dimensional distribution of δ_{iso} and C_Q extracted from the experimental spectrum, with all MD-GIPAW data and mean values with respect to the oxygen coordination number, respectively. (c) MAS spectra.

configuration for Na but with non negligible content of 5 and 8-fold environment.

Conclusions

The results obtained by the application of the synergic approach used in this work which combines experimental and theoretical elaboration of solid-state MAS ^{29}Si, ^{31}P, ^{23}Na, and ^{17}O and ^{23}Na 3QMAS NMR spectra add new important insights into the atomic level structure of the 45S5 Bioglass.

In particular, they furnished some help in answering to three questions regarding (a) the Q^n distribution of silicon; (b) the presence of Si−O−P bridges, mainly postulated by MD simulations; and (c) the degree of randomness of the distribution of Na and Ca ions around NBO and BO oxygen atoms.

The structural factors listed above are fundamental points from the biomedical point of view since they control the reactivity of the implanted material in body fluids, and can be changed by rational design of glass compositions to optimize biodegradation and bioactivity.

An excellent agreement has been found between the theoretical NMR spectra and the experimental data, allowing the validation of the whole approach adopted in this work which encompasses (a) the 3D structural models obtained by CMD simulations, (b) the structure relaxation and NMR parameters calculations at the DFT/GIPAW level, and (c) the generation of the solid-state MAS ^{29}Si, ^{31}P, ^{23}Na, and ^{17}O and ^{23}Na 3QMAS NMR spectra by means of the fpNMR code. To the best of our knowledge, this is the first time that the ^{17}O 3QMAS NMR spectrum of a mixed-alkali glass is reproduced with high accuracy by means of MD simulations.

Moreover, the ^{17}O MQMAS spectrum of 45S5 Bioglass, experimentally collected for the first time, has been quantitatively analyzed by a direct fit providing the resolution of all the structural groups contributing to the glass structure. The Si−NBO/Si−BO−Si ratio determined by the glass composition and theoretical NMR parameters have been used to guide the fit of the experimental ^{29}Si MAS spectrum. The latter suggests that the host silica network consists of chains and rings of Q^2 (67.2%) SiO_4 tetrahedra cross-linked by Q^3 (22.3%) species and terminated by a low quantity of Q^1 (10.5%) species.

The ^{31}P NMR indicates that phosphorus is present as isolated PO_4 units in the structure, which subtract sodium and calcium cations from a network modifying role in the silicate network. No Si−O−P bridging are present in the glass as evidenced by ^{31}P static, MAS, and ^{17}O 3QMAS NMR.

Finally, both the experimental and theoretical results agree in highlighting a nonrandom distribution for the modifier ions (Na, Ca) surrounding Si−NBO and P−NBO sites.

Acknowledgment. Some of the authors thank the Italian Ministry of University and Research for funding (Project COFIN2008, prot. 2008J9RNB3 "Integrazione Temporale per l'Evoluzione Molecolare") and CINECA (www.cineca.it) for computational resourses. A.P. also thanks Telecom Italia for financial support. Part of this work (T.C.) was performed using the HPC resources from GENCI-CCRT (Grant gen6303).

Supporting Information Available: Derivation of constraints for the analysis of ^{17}O MQMAS and ^{29}Si MAS NMR spectra, and formulae for the calculation of random distribution of Na and Ca around oxygen atoms (PDF). This material is available free of charge via the Internet at http://pubs.acs.org.